^{18}F-EF5: A New PET Tracer for Imaging Hypoxia in Head and Neck Cancer

Gaber Komar[1], Marko Seppänen[1], Olli Eskola[1], Paula Lindholm[2], Tove J. Grönroos[1], Sarita Forsback[1], Hannu Sipilä[1], Sydney M. Evans[3], Olof Solin[1], and Heikki Minn[1,2]

[1]Turku PET Centre, Turku, Finland; [2]Department of Oncology and Radiotherapy, University of Turku, Turku, Finland; and [3]Department of Radiation Oncology, School of Medicine, University of Pennsylvania, Philadelphia, Pennsylvania

The aim of this study was to evaluate 2-(2-nitro-^{1}H-imidazol-1-yl)-*N*-(2,2,3,3,3-pentafluoropropyl)-acetamide (EF5) labeled with ^{18}F-fluorine to image hypoxia in patients with squamous cell carcinoma of the head and neck (HNSCC). **Methods:** Fifteen patients with HNSCC were studied. Measurement of tumor blood flow was followed by an ^{18}F-EF5 PET/CT scan. On a separate day, ^{18}F-FDG PET/CT was performed to determine the metabolically active tumor volume. In 6 patients, dynamic ^{18}F-EF5 images of the head and neck area were acquired, followed by static images acquired at 1, 2, and 3 h after injection. In the remaining 9 patients, only static images were obtained. ^{18}F-EF5 uptake in tumors was compared with that in neck muscle, and the ^{18}F-EF5 findings were correlated with the ^{18}F-FDG PET/CT studies. **Results:** A total of 13 primary tumors and 5 lymph node metastases were evaluated for their uptake of ^{18}F-EF5. The median tumor-to-muscle ^{18}F-EF5 uptake ratio (T/M) increased over time and was 1.38 (range, 1.1–3.2) 3 h after tracer injection. The median blood flow in tumors was 36.7 mL/100 g/min (range, 23.3–78.6 mL/100 g/min). Voxel-by-voxel analysis of coregistered blood flow and ^{18}F-EF5 images revealed a distinct pattern, resulting in a T/M of 1.5 at 3 h to be chosen as a cutoff for clinically significant hypoxia. Fourteen of 18 tumors (78%) had subvolumes within the metabolically active tumor volumes with T/M greater than or equal to 1.5. **Conclusion:** On the basis of these data, the potential of ^{18}F-EF5 to detect hypoxia in HNSCC is encouraging. Further development of ^{18}F-EF5 for eventual targeting of antihypoxia therapies is warranted.

Key Words: head and neck cancer; hypoxia; ^{18}F-EF5; squamous cell carcinoma

J Nucl Med 2008; 49:1944–1951
DOI: 10.2967/jnumed.108.053785

Since the classic study by Thomlinson and Gray in 1955 (*1*), hypoxia has emerged as one of the key factors in malignant tumor aggression and progression and as a crucial obstacle to local and distant control of malignant diseases (*2,3*). The presence of hypoxia is associated with a more aggressive tumor phenotype, resulting in local tissue invasion and increased metastatic potential (*4*). In addition to its role as a major cause of failure of both radiation therapy and chemotherapy, many studies have confirmed the presence of hypoxia as an independent negative prognostic factor for patient outcome in various tumor histologies (*5,6*).

Polarographic electrode studies were the first method to demonstrate the presence of hypoxia in human tumors (*7*). This invasive technique has both logistic and technical limitations, which prevent its routine use in the clinical setting (*8*). The analysis of binding of the 2 currently used exogenous markers of clinical relevance, pimonidazole and 2-(2-nitro-^{1}H-imidazol-1-yl)-*N*-(2,2,3,3,3-pentafluoropropyl)-acetamide (EF5), is based on tissue biopsies and is also invasive. Binding of both of these agents has been shown to predict outcome in patients with head and neck cancer (*9,10*); however, clinically applicable methods for specifically identifying hypoxic regions in tumors and, more important, overcoming the negative effects on treatment modalities of these methods have yet to be described (*11*).

Recently, PET imaging has become a promising tool for detecting hypoxia, and several PET tracers have emerged for this purpose (*12*). However, none of the clinically tested ^{18}F-labeled 2-nitroimidazole tracers that fulfill all of the requirements of a positron-emitting hypoxia marker has been generally accepted for clinical purposes. ^{18}F-fluoromisonidazole (^{18}F-FMISO) (*13*), ^{18}F-fluoroerythronitroimidazole (*14*), ^{18}F-fluoroazomycin arabinoside (*15*), and ^{18}F-fluoroetanidazole have been used with varying success as PET probes for hypoxia imaging, but only ^{18}F-FMISO is available in more than a few of the centers worldwide. However, a new group of etanidazole-based compounds, >2-(2-nitroimidazol-^{1}H-y)-*N*-(3-flouropropyl)acetamide (EF1) (*16*), 2-(2-nitroimidazol-^{1}H-y)-*N*-(3,3,3-tryflouropropyl)acetamide (EF3), and EF5 (*17–19*), has been developed both as biopsy-based (*20*) and as PET-based agents, and ^{18}F-EF5 has been synthesized by Dolbier et al. (*17*) as well as at our center.

As indicated above, EF5 has been extensively studied in rodent and human tumors, in normal tissues, and in nonneoplastic pathologic processes (*21*). In addition to the clinical trial in squamous cell carcinoma of head and neck (HNSCC), immunohistochemistry-based assays of EF5

Received Apr. 24, 2008; revision accepted Aug. 14, 2008.
For correspondence or reprints contact: Gaber Komar, Turku PET Centre, P.O. Box 52, FIN-20521, Turku, Finland.
E-mail: gaber.komar@tyks.fi

have been shown to be associated with aggression in malignant glioma (*22,23*) and in sarcomas (*24*).

In the present study, we used ^{18}F-EF5 as a hypoxia imaging agent in patients with HNSCC and characterized the time course of uptake of intravenously injected ^{18}F-EF5 in the head and neck area to determine the most suitable PET protocol for this tracer. All patients were also scanned using ^{15}O-water (^{15}O-H_2O) to determine tumor blood flow, and a 2-^{18}F-FDG PET scan was performed on a separate day to determine the metabolically active tumor volume. By comparing blood flow with regional uptake of ^{18}F-EF5, we studied the potential of the tracer for noninvasive detection of hypoxia with PET.

MATERIALS AND METHODS

Patient Population

The study was performed after it was approved by the Ethical Board of Turku University Central Hospital and in accordance with the Helsinki Declaration. Informed consent was obtained from each patient. Fifteen patients (11 men, 4 women) with newly diagnosed HNSCC, referred to Turku University Central Hospital for chemoradiotherapy between December 2005 and January 2007, participated in this study. The average patient age was 55.5 ± 14 y (range, 24–77 y) and the average body mass was 75.9 ± 20.9 kg (range, 52–129 kg). Relevant patient information is presented in Table 1.

Synthesis of ^{18}F-EF5 and ^{18}F-FDG

^{18}F-EF5 was synthesized from 2-(2-nitro-^{1}H-imidazol-1-yl)-*N*-(2,3,3-trifluoroallyl)-acetamide using high-specific-radioactivity ^{18}F-F_2 as the labeling reagent (*25*). The specific radioactivity of ^{18}F-EF5, decay-corrected to the end of synthesis, exceeded 3.7 GBq/μmol. Radiochemical purity was higher than 98.5% in every production. A more detailed description of ^{18}F-EF5 synthesis will be reported elsewhere.

^{18}F-FDG was synthesized from mannosyl triflate using a nucleophilic method. Radiochemical purity exceeded 95%, and specific radioactivity was approximately 74 GBq/μmol at the end of synthesis.

Synthesis of ^{15}O-H_2O

A low-energy deuteron accelerator Cyclone 3 (IBA Molecular) was used for production of ^{15}O. To synthesize radiowater for blood flow imaging, a diffusion membrane technique in a constantly working water module was applied (Radio Water Generator; Hidex Oy). For each examination, the radioactivity of products was recorded online using a low-voltage ionization chamber.

PET/CT Device

All data were acquired on a Discovery STE PET/CT scanner (GE Healthcare), which combined a helical 16-slice CT scanner and a BGO block PET tomograph. The PET scanner comprised thirteen 440 BGO crystals arranged in 24 rings, yielding 47 transverse slices spaced axially by 3.27 mm. The PET field of view was 70 cm in diameter and 15.7 cm in axial length. Attenuation correction was performed using a low-dose ultra-fast CT protocol (80 mAs, 140 kV, and 0.3 mSv per field of view).

Data Acquisition Protocol

Measurement of tumor blood flow with ^{15}O-H_2O was followed by PET/CT with ^{18}F-EF5. ^{18}F-FDG PET/CT was performed on a separate day. Both studies were performed in random order, within an average of 6 d (range, 1−16 d). The sequence of events for the combined ^{15}O-H_2O/^{18}F-EF5 study is shown in Figure 1. All patients fasted for at least 6 h before tracer injection. A venous line was inserted into the patient's forearm for injection of the tracer, and another catheter was placed in the contralateral radial artery for the frequent blood sampling during the image acquisition. Patients were positioned supine on the tomograph couch, with their arms alongside their body; a head support (combined ^{15}O-H_2O and ^{18}F-EF5 study) or a custom-made thermoplast mask used in radiotherapy (^{18}F-FDG study) stabilized the head.

TABLE 1
Patient Characteristics

Patient no.	Sex	Age (y)	Weight (kg)	BMI	Tumor site	Stage			UICC stage
						T	N	M	
1	M	45	65	21.2	Base of tongue (oropharynx)	T4	N0	M0	IVA
2	M	58	72	24.3	Retromolar trigonum (oropharynx)	T2	N1	M0	III
3	F	58	50	21.6	Tonsil (oropharynx)	T1	N2b	M0	IVA
4	M	62	67	22.4	Supraglottic (larynx)	T2	N2b	M0	IVA
5	F	39	68	21.5	Supraglottic (larynx)	T4	N2c	M0	IVA
6	M	43	100	27.7	Upper gingiva (oral cavity)	T4	N1	M0	IVA
7	M	68	70	26.0	Base of tongue (oropharynx)	T2	N1	M0	III
8	F	46	59	22.5	Nasopharynx (nasopharynx)	T1	N2c	M0	III
9	M	53	76	24.8	Glottic (larynx)	T4	N1	M0	IVA
10	M	24	129	39.8	Mobile tongue (oral cavity)	T3	N2b	M0	IVA
11	M	70	92	27.8	Floor of mouth (oral cavity)	T1	N0	M0	I
12	M	57	77	25.7	Base of tongue (oropharynx)	T1	N2a	M0	IVA
13	M	65	98	29.6	Nasopharynx (nasopharynx)	T2a	N1	M0	IIB
14	M	67	64	22.7	Base of tongue (oropharynx)	T1	N2b	M0	IVA
15	F	77	52	22.2	Maxillary sinus	T4	N1	M0	IVA

BMI = Body Mass Index; UICC = International Union Against Cancer.

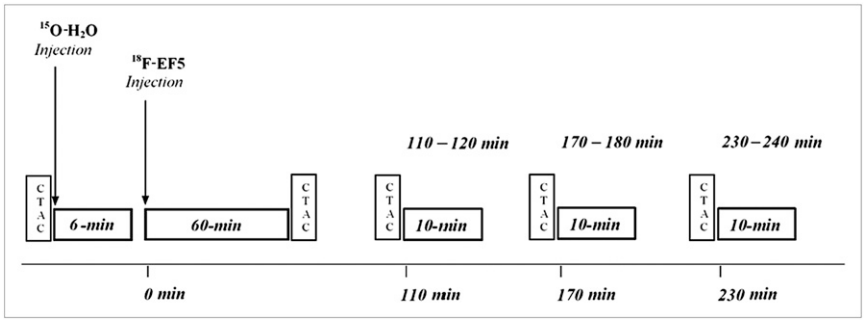

FIGURE 1. Time course for scanning protocol of combined ^{15}O-H_2O and ^{18}F-EF5 study. CTAC = computer-assisted tomography for attenuation correction.

The study began with a CT scan, followed by an injection of ^{15}O-H_2O (median dose, 1,205 MBq or 16.8 ± 3.2 MBq/kg) and an immediate 6-min dynamic emission image acquisition. Arterial blood was withdrawn with a pump (Alitea C-4V; Alitea AB) at a speed of 6 mL/min to obtain the input function. Blood radioactivity was measured with an online detector (Advance Fluid Radioactivity Quantifier; GE Healthcare). After the completion of the ^{15}O-H_2O blood flow study, a slow (~15 s) bolus of ^{18}F-EF5 was injected (median dose, 250 MBq or 3.9 ± 1.5 MBq/kg). For 6 of the 15 patients, we acquired a set of dynamic images over a 60-min period after the tracer injection to demonstrate the early tracer distribution; patients were then removed from the scanner. Late images (2 frames of 300 s) were acquired at 2, 3, and 4 h after the tracer injection. Patients were allowed to relax quietly in the preparation room between these late acquisitions.

During the ^{18}F-EF5 image acquisition, 28 blood samples were obtained through the arterial catheter to measure the time course of tracer concentration and presence of any tracer metabolites in plasma. A total of 9, 14, 15, and 3 images were acquired at 1, 2, 3, and 4 h after injection, respectively.

The ^{18}F-FDG study was performed according to the routine ^{18}F-FDG protocol used for radiotherapy planning in our center. The median injected ^{18}F-FDG dose was 369 MBq (4.8 ± 0.9 MBq/kg).

Image Analysis

Calculation of Metabolically Active Tumor Volume (MATV), Hypoxic Subvolume, and Percentage Hypoxic Area (PHA). The manufacturer's proprietary software (Advanced Workstation 4.3; GE Healthcare) was used for the analysis of tumor volumes, analysis of uptake volumes for ^{18}F-FDG and ^{18}F-EF5 tracers, and calculation of PHA.

For ^{18}F-FDG images, MATV was identified visually on the basis of anatomic CT guidance and ^{18}F-FDG accumulation. Three-dimensional regions of interest (ROIs) were positioned to cover the entire ^{18}F-FDG–avid volume of the uptake region. These ROIs were drawn manually in all planes in which the accumulation was visible and then automatically summed to create one 3-dimensional ROI and obtain the metabolically active tumor volume.

For ^{18}F-EF5 images, ROIs generated from the ^{18}F-FDG study were transferred to the combined blood flow and ^{18}F-EF5 study by carefully aligning the corresponding image planes of the 2 PET/CT acquisitions using noncommercial research imaging software (Vinci, Max-Planck-Institut für Neurologische Forschung; http://www.mpifnf.de/vinci/). Using this software, we were able to draw equally sized ROIs and position them in the same portion of the tumor in images obtained with all 3 tracers. ^{18}F-EF5 tumor-to-muscle uptake ratios (T/M) at 1, 2, and 3 h were determined as the ratio between the resulting 3-dimensional tumor ROI and a large ROI covering a dorsal neck muscle area contralateral to the tumor in 3 consecutive planes. Maximum T/M for all time points was defined by comparing the highest activity in a tumor ROI with a whole-muscle ROI. In the 6 patients receiving dynamic ^{18}F-EF5 scans, the same ROIs were applied throughout the long acquisition protocol. The ^{18}F-EF5–avid volume at 3 h was determined using 3 arbitrarily selected T/M thresholds: 1.4, 1.5, and 1.6, which were evaluated against the voxel-by-voxel correlation between the blood flow and ^{18}F-EF5 images. The thresholds formed cutoff values for 3-dimensional tumor regions presumably presenting significant hypoxia within the MATV. The PHA was calculated by dividing the summed volume of voxels above the selected T/M threshold by the MATV.

Calculation of Blood Flow. Blood flow images were calculated using a 1-tissue-compartment model, which was linearized (*26*). Lawson–Hanson nonnegative least-squares analysis was used to solve general linear least-squares functions. The input function for the tissue was corrected for the measured external dispersion in the tubing by deconvolution with an exponential function. The delay was corrected by fitting the input curve into the measured tissue curve (*27,28*).

Analysis of Blood Flow Images; Correlation Between ^{15}O-H_2O, ^{18}F-EF5, and ^{18}F-FDG; and Time Course of ^{18}F-EF5 Uptake. A comparative analysis of the global uptake of the tracers in the corresponding regions of tumors was performed with the Vinci software. The size and location of the ROIs was important in this comparative analysis, because a larger (MATV/^{18}F-FDG–sized) ROI in ^{18}F-EF5 and ^{15}O-H_2O images would result in much lower average values. Under these circumstances, the information regarding the potentially different localization of high-uptake areas inside the tumor could not be accurately extracted. An ROI was, therefore, drawn according to visible ^{18}F-EF5 uptake and then copied onto ^{18}F-FDG and ^{15}O-H_2O images for each patient. In the instance in which no visible subregion of ^{18}F-EF5 was discernable, the ^{18}F-FDG image was used to determine the size and position of the ROI in ^{18}F-EF5 and ^{15}O-H_2O images.

Voxel-by-voxel analysis was also performed to determine the relationship between spatial distributions of tumor blood flow as measured by the ^{15}O-H_2O scan and ^{18}F-EF5 uptake presumably representing hypoxia. The colocalization of blood flow and hypoxia images was the primary method used to validate an appropriate threshold for calculation of PHA. The voxel-by-voxel analysis was performed using the image analysis tool AMIDE (*29*). Both blood flow and hypoxia images were carefully aligned using the CT image, and an identical ROI covering the whole tumor was positioned on both images. The individual voxel values (including the localization information) were extracted from both

images, and the values for each voxel were compared. ^{18}F-EF5 tumor values were divided by the average ^{18}F-EF5 muscle value of the respective image to obtain T/M ratios for each voxel. Voxel values for both tracers, including all 18 lesions, were plotted on 1 graph to obtain an expression of the relationship between blood flow and hypoxia in HNSCC, as evaluated with ^{15}O-H_2O and ^{18}F-EF5 PET.

Statistical Analysis. The Student *t* test was used to test the difference between the ^{18}F-EF5 standardized uptake values at different times. A Pearson correlation coefficient was calculated to test the correlation between the uptake values of different tracers.

RESULTS

In 15 patients, a total of 18 lesions were identified, and these were further analyzed. These lesions included 13 primary tumors and 5 lymph node metastases. In patient 2, only the lymph nodes could be imaged because the primary tumor was excised before scanning. Additionally, in patient 12, a radiologically and clinically undetectable (but histologically confirmed) mass, designated as a T1 lesion in the base of the tongue, was not seen on the ^{18}F-FDG scan (nor the ^{18}F-EF5 scan) and was therefore excluded from quantitative analysis. Furthermore, ^{18}F-FDG–positive lymph node metastases measuring less than 1 cm in 4 patients were considered too small for quantitative analysis, and 4 more patients had undetectable nodal micrometastases found only at elective neck dissection after radiotherapy.

Dynamics of ^{18}F-EF5 Uptake

In the early phase (minutes after injection), we observed a pattern in the ^{18}F-EF5 uptake resembling the ^{15}O-H_2O blood flow images. This was most likely due to the high concentration of the tracer in the blood and consequently also in the hyperperfused areas of the tumors. The activity in these areas decreased over time, and a slow but steady increase of the activity in other tumor regions became visible (Fig. 2). We also observed a similar early stage, presumably blood flow–dependent, pattern in tumors that did not show ^{18}F-EF5 uptake at later time points.

To determine the optimal imaging time point, we compared the ^{18}F-EF5 T/M for all the static-emission image-acquisition time points after injection (1, 2, and 3 h; Fig. 3A). Because of a steady increase of T/M values from 1 to 2 h (mean T/M, $P = 0.005$; max T/M, $P < 0.001$) and from 2 to 3 h (mean T/M, $P = 0.01$; max T/M, $P = 0.005$), a decision was made to scan 3 additional patients at 4 h after injection. In these 3 patients, we observed a small decrease of the mean T/M ratio ($P = 0.29$), a small increase of the max T/M ratio when compared with 3-h images ($P = 0.32$; Fig. 3B), and a noticeable degradation of overall image quality.

Comparison of ^{18}F-EF5, ^{18}F-FDG, and ^{15}O-H_2O

In all patients except patient 12, the primary or metastatic lesion was clearly visible on both the blood flow (^{15}O-H_2O) and the ^{18}F-FDG images (Fig. 4). The lesion uptake values for ^{18}F-FDG, blood flow, and ^{18}F-EF5 at 3 h after injection are shown in Table 2. The global tumor uptake did not show a significant correlation between any of the 3 tracers, although the patterns of regional uptake in the blood flow and early ^{18}F-EF5 images were similar. Voxel-by-voxel analysis revealed a complex picture of the relationship between tumor blood flow and tumor hypoxia, as monitored by ^{18}F-EF5. Three visually distinct trends were observed. All regions with high blood flow had a T/M less than 1.5 (Fig. 5, region A) and displayed a positive correlation between blood flow and ^{18}F-EF5 T/M ($r = 0.621$, $P < 0.0001$). In regions with blood flow values less than, for example, 30 mL/100 g/min (Fig. 5, region B), we observed a negative correlation ($r = -0.042$, $P = 0.259$) between blood flow and ^{18}F-EF5 T/M. Between these 2 expected extremes (Fig. 5, region C), blood flow and hypoxia increased at approximately the same rate ($r = 0.295$, $P < 0.0001$). Analysis of all the tumor voxel values above T/M equal to 1 showed an inverse relationship between the 2 tracers ($r = -0.2$).

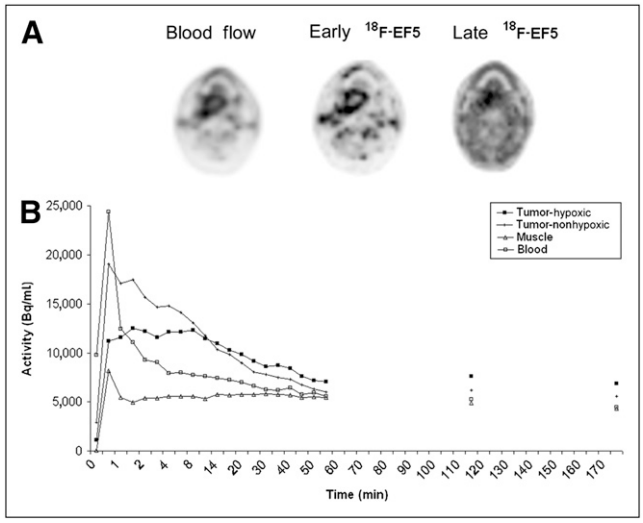

FIGURE 2. (A) Combined blood flow and early and late (3 h from injection) ^{18}F-EF5 images in patient 1, who presented with right T4N0 base-of-tongue HNSCC. Note similarity of blood flow and early ^{18}F-EF5 images (2 min from injection), showing doughnutlike appearance of tracer uptake in tumor. By contrast, ^{18}F-EF5 image obtained 3 h after injection shows uptake in central, less perfused area. (B) Time–activity curves from same tumor as in A, demonstrating differential uptake kinetics of ^{18}F-EF5 of peripheral (nonhypoxic) and central (hypoxic) parts of tumor. In well-perfused area, initial uptake of ^{18}F-EF5 is higher than that in more hypoxic area; after first 15 min, reverse is true. With exception of first 90-s image, uptake in dorsal neck muscle and arterial blood remain lower than that in both tumor parts throughout 3-h acquisition time.

PHA

To determine the MATV, a paint tool was used, and the entire visible tumor was selected in all planes and summed. The average measured MATV was 9.02 cm^3 (0.4–55.35 cm^3). Because of the lack of previous clinical experiences using ^{18}F-EF5, 3 T/M thresholds were applied in the ^{18}F-EF5 images.

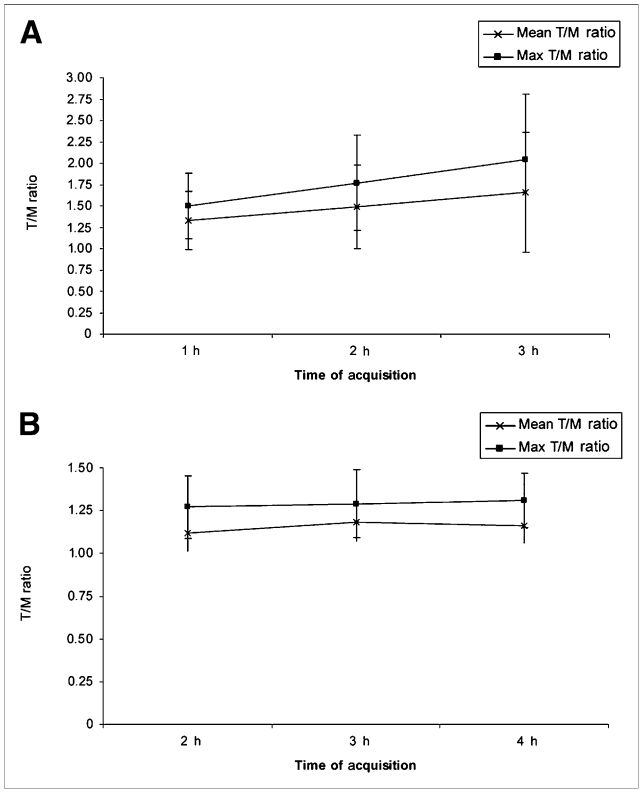

FIGURE 3. Maximum and mean ^{18}F-EF5 T/M ratios over all static emission image acquisition time points. (A) Mean T/M ratios increase from 1 through 3 h after injection. (B) Higher maximum T/M ratio and lower mean T/M ratio at 4 h after injection, when compared with 3 h after injection, could be explained by increasing image noise (and decreasing overall image quality).

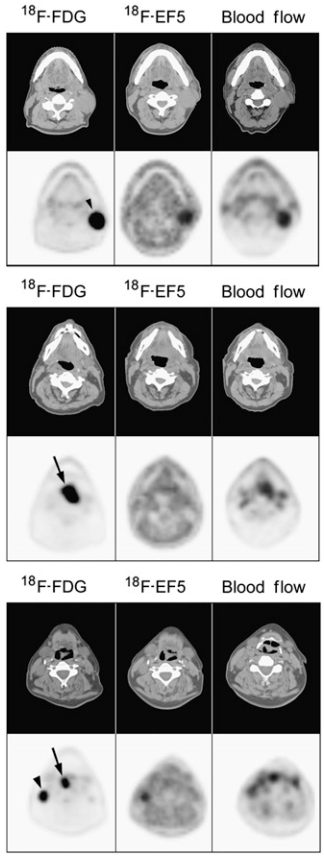

FIGURE 4. Examples of both PET and CT images for all 3 tracers for 3 patients. ^{18}F-EF5 images are made at 3 h after injection. Arrows indicate primary tumors, and arrowheads indicate metastatic lesions.

The volumes composed of voxels above this threshold were considered hypoxic, and these volumes varied with the applied thresholds (Fig. 6). The lowest threshold of 1.4 resulted in the largest PHA (average PHA, 48.9%; range, 25%−97%) such that 14 of 18 tumors (78%) displayed some degree of hypoxia. As expected, these values decreased with the increased thresholds. For the threshold of 1.5, the average PHA was 30.5% (range, 8%−87%), and the percentage of hypoxic tumors remained at 78%. With the highest threshold of 1.6, the average PHA dropped to 16% (range, 1%−74%), and areas above this threshold were found in 11 of 18 lesions (61%). Comparison of individual thresholds with the blood flow data depicted in Figure 5 supported a T/M threshold of 1.5 to represent clinically significant hypoxia, because all tumor regions with high blood flow fell below this value.

In lesions with areas above the T/M ratio of 1.5, a correlation between the size of the lesion and the PHA was not observed.

DISCUSSION

In our study, patients with untreated HNSCC were studied with the novel tracer ^{18}F-EF5 as a hypoxia imaging agent. Our data corresponded to previously published results in cells, animals, and humans using quantitative immunohistochemical detection of non–^{18}F-labeled EF5 (*9,30*) and supported our hypothesis that ^{18}F-EF5 would be an accurate PET marker of hypoxia, with uniform access to all tissues, dominantly excreted via the kidneys and with no detectable metabolism. These observations had been previously confirmed in preclinical studies conducted by Grönroos et al. in which an almost complete absence of ^{18}F-EF5 metabolites in the blood was demonstrated (*31*). On the basis of these preclinical PET studies and many studies on the immunohistochemical detection of EF5, we predicted that ^{18}F-EF5 would display favorable biokinetic properties as a PET tracer to be used in humans (*18,32*). Because there was limited information on uptake of ^{18}F-EF5 in human tissues, our study included a long scanning protocol. Specifically, we sought to determine an optimal time point for detection of specific binding in hypoxic tissues and predicted that 2–4 h from injection would be optimal based on previous data from other 2-nitroimidazole compounds. Our data, showing increasing T/M over the first 3 h and slight degradation of the image quality at 4 h, support the recommendation that 3 h after the ^{18}F-EF5 injection is the optimal acquisition time for clinical protocols.

In addition to ^{18}F-EF5 imaging, blood flow studies with ^{15}O-H_2O and ^{18}F-FDG imaging were performed to evaluate the interrelationship between tumor blood flow and metabolic activity. The measured blood flow values for tumors were significantly higher than those found in muscles of adjacent

TABLE 2
Tumor Blood Flow and Uptake of ^{18}F-FDG and ^{18}F-EF5

Patient no.	Blood flow (mL/100 g/min)	Uptake of ^{18}F-FDG		Uptake of ^{18}F-EF5 3 h after injection		
		Max SUV	Mean SUV	Mean T/M	Max T/M	PHA
1	54.84	4.80	3.74	1.49	1.75	34.7
2 LN*	78.55	4.13	2.53	1.20	1.39	0
3	70.72	12.67	8.58	1.05	1.15	0
4	28.09	5.35	2.33	1.27	1.52	66.7
5	39.64	22.06	14.08	1.20	1.20	0
6	36.69	5.71	2.70	1.46	1.64	29.9
7	52.33	10.84	7.69	1.21	1.35	0
LN	35.26	8.39	6.33	1.84	2.29	64.3
8	25.92	6.35	4.74	1.38	1.74	7.6
LN	43.53	5.17	3.67	1.37	1.62	8
9	23.26	7.98	6.49	3.34	4.07	86.8
LN	30.96	5.45	3.93	1.90	2.63	44.9
10	40.24	10.56	7.16	1.51	1.90	20.8
LN	29.66	8.48	4.68	1.37	1.74	34.5
11	31.87	4.56	3.56	1.33	1.65	11.1
12	30.96	7.46	4.90	1.37	1.91	40
13	49.56	9.12	7.68	1.76	2.02	50.4
14	†	8.66	6.10	1.70	2.26	49,3

*Patient 2 had primary tumor excised before scanning.
†Input curve was lost because of technical difficulties.
SUV = standardized uptake value; PHA = percentage hypoxic area (SUV) of ^{18}F-FDG, and hypoxic fraction (PHA) as percentage of voxels above T/M = 1.5 3 h after injection of ^{18}F-EF5.
LN designates lymph node metastasis of preceding patient. Metabolism is expressed as SUV.

neck areas, varying between 23 and 78 mL/100 g/min, and the muscle values remained considerably lower (between 2.5 and 12 mL/100 g/min). These results are in accordance with previous studies of HNSCC performed at our center (*33*).

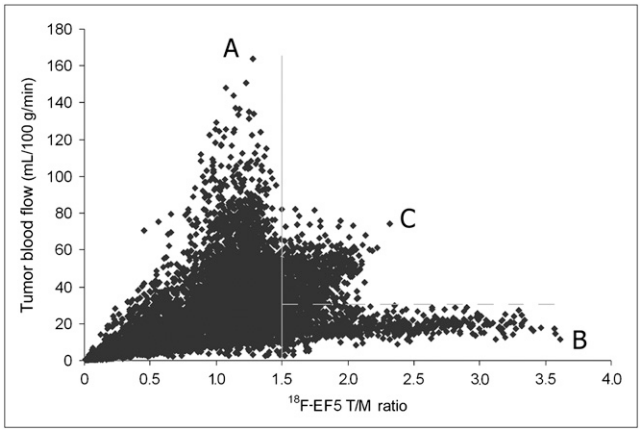

FIGURE 5. Relationship between uptake of ^{18}F-EF5 at 3 h expressed as T/M and blood flow on voxel-by-voxel basis in all 18 primary and metastatic tumors. *y*-Axis indicates threshold value of 1.5, tentatively representing PHA. *x*-Axis indicates perfusion value of 30 mL/100 g/min, which represents border between poorly and well-perfused areas. Resulting are areas of high perfusion with good oxygenation (trend A), low perfusion with low oxygenation (trend B), and intermediate perfusion (trend C).

To validate ^{18}F-EF5 as a hypoxia marker, we compared both global and regional blood flow in tumors with the uptake of the radiolabeled 2-nitroimidazole during early and late phases of biodistribution. Both ^{18}F-FMISO and ^{18}F-fluoroerythronitroimidazole show some degree of positive correlation with blood flow within the first minutes after injection; this was the case for ^{18}F-EF5 as well (*33*). In 12 of 15 patients ^{18}F-EF5 distribution changed over time from highly perfused into less perfused areas of the tumor. This is in accordance with the cumulative character of covalent binding of ^{18}F-EF5 in hypoxic cells, which is typical for all 2-nitroimidazole–based compounds. As expected,

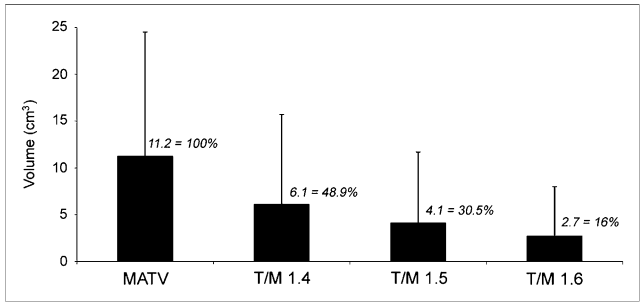

FIGURE 6. Comparison of percentages of tumor subvolumes representing PHA using 3 different T/M ^{18}F-EF5 uptake threshold values. MATV is determined from ^{18}F-FDG study performed on separate day.

global blood flow did not show any distinct relationship with uptake of ^{18}F-EF5 during the period of hypoxia-specific binding. We, therefore, performed a voxel-by-voxel analysis for evaluation of regional differences in blood flow and hypoxia 3 h after injection of ^{18}F-EF5. During this time, regions of several tumors showed high uptake, consistent with the presence of hypoxia. The cumulative findings from all 18 tumors showed a striking correlation between blood flow and hypoxia (Fig. 5). Under circumstances of low blood flow and high ^{18}F-EF5 binding (hypoxia) and high blood flow and low ^{18}F-EF5 binding (oxia), a clear inverse correlation could be seen; the slope of the best-fit lines for these relationships was significantly different. Interestingly, in tumor regions in which the ^{18}F-EF5 T/M was between 1.5 and 2.2, a relationship with an intermediate slope was identified (Fig. 5), in which slightly increased blood flow and moderate PET values were observed.

Because all tumor regions with high blood flow fell below an ^{18}F-EF5 T/M of 1.5, we proposed this level as a cutoff for determination of PHA. This T/M value as an indicator of significant hypoxia in head and neck cancer (and other tumor types) needs further validation, especially in outcome studies, before it can be generally accepted. The intermediate zone in our study suggests a more complex and heterogeneous relationship between blood flow and hypoxia and may signify the presence of hypoxia in some well-perfused tumor regions. Several biologic explanations for this phenomenon have been proposed, including acute changes in blood flow, plasma flow without red blood cells, retrograde flow, longitudinal gradients, and flow in arteriovenous malformations. Interestingly, a similar observation was made by Thorwarth et al., who used ^{18}F-FMISO to evaluate both blood flow and hypoxia at the same time point but used data-modeling approaches different from those described in this study (*34*).

The uptake of ^{18}F-EF5 did not correlate with that of ^{18}F-FDG. This was particularly obvious in some patients with several ^{18}F-FDG–avid lesions of which only 1 showed uptake of ^{18}F-EF5 (Fig. 4). This lack of correlation is undoubtedly due to multiple uptake mechanisms of ^{18}F-FDG, most of which do not depend on oxygen concentration (*35*). Our findings, however, do underline the importance of ^{18}F-FDG for planning of radiation therapy in head and neck (and likely other) cancers.

We also observed a lack of correlation between uptake of ^{18}F-EF5 in the primary tumor and the metastatic lymph nodes. Similar results have been obtained with other noninvasive hypoxia markers including ^{18}F-FMISO and ^{18}F-fluoroazomycin arabinoside. This is in contradiction to a report on correlation between the oxygenation status of the primary tumor and that of the metastatic lymph nodes using biopsy-based methods (*36*).

The primary purpose of this study was to demonstrate the potential of PET ^{18}F-EF5 for evaluating hypoxia in previously untreated head and neck cancer. Our initial findings support the hypothesis that ^{18}F-EF5 provides high T/M ratios in a subset of patients with HNSCC and that it has a generally inverse relationship with blood flow. These data take their place next to other hypoxia-avid PET tracers such as ^{18}F-FMISO (*37*) and ^{18}F-fluoroazomycin arabinoside (*15*), and future studies will determine the advantages and disadvantages of each of these agents. It is possible that certain agents will perform differently in specific tumor types. One clear advantage of ^{18}F-EF5 is that it is the same molecule as EF5, which has been used extensively to study hypoxia in numerous clinical and preclinical settings (*17–20,22,31,32,38*). It is our goal to compare results from studies in which EF5-based immunohistochemical images were compared with PET ^{18}F-EF5 images. Such studies will help clarify our suggestion that a T/M equaling 1.5 is a relevant threshold for clinically significant hypoxia. In a large multicenter study of head and neck lymph node metastases, Nordsmark et al. found that the fraction of pO_2 values less than or equal to 2.5 mm Hg, measured using the Eppendorf method, was the only statistically significant parameter for the patient prognosis. The average fraction of tumor volume with values above this threshold was found to be 19%, which roughly corresponds to an ^{18}F-EF5–avid fraction of 16% obtained by using a T/M threshold of 1.6. This, of course, is not sufficient to conclude that a T/M of 1.6 corresponds to a pO_2 cutoff value of less than or equal to 2.5 mm Hg, bearing in mind the caveats of comparing noninvasive and invasive methods. These data are preliminary, and additional studies will be necessary to fully validate that a T/M ratio of 1.5 is an appropriate measure of significant hypoxia. A formal comparison between characteristics of other tracers and those of ^{18}F-EF5 will be easier to perform using this cutoff as a starting point. A T/M of 1.5 (Fig. 5) in ^{18}F-EF5 PET in patients with HNSCC to measure hypoxia is a reasonable starting point in studies in which outcome- and hypoxia-targeted therapies are being evaluated.

CONCLUSION

We presented the first, to our knowledge, human study of the ^{18}F-EF5 PET hypoxia marker ^{18}F-EF5. We compared uptake of ^{18}F-EF5 with blood flow as measured by radioactive water and metabolism measured with ^{18}F-FDG in patients with HNSCC. The data support the idea that the initial uptake of ^{18}F-EF5 is governed by blood flow; in the later phase, uptake and binding are hypoxia-specific. The ^{18}F-EF5 binding distributions and patterns in primary tumors and cervical lymph node metastases are heterogeneous, which is consistent with clinical expectations and previously published data using immunohistochemical analyses of EF5. Uptake of ^{18}F-EF5 increased until 3 h after injection, after which time the quality of the image decreased. We propose that the 3-h time point is the optimal time for detecting hypoxia-specific binding in human head and neck cancer. By comparing regional blood flow and ^{18}F-EF5 T/M at 3 h, we identified a T/M equal to 1.5 as an appropriate threshold for determining the presence of clin-

ically significant hypoxia. Our future studies include evaluation of ^{18}F-EF5 PET as a prognostic marker for outcome studies in this patient group.

ACKNOWLEDGMENTS

We thank all the staff at the Turku PET Centre, the Department of Oncology and Radiotherapy, and the Department of Otorhinolaryngology for help in various phases of this project. The study was supported in part by the European Union's FP6 Commission BioCare (Molecular Imaging for Biologically Optimized Cancer Therapy), under contract 505785. Additional funding has been obtained from The Finnish Cancer Organization.

REFERENCES

1. Thomlinson RH, Gray LH. The histological structure of some human lung cancers and the possible implications for radiotherapy. *Br J Cancer.* 1955;9:539–549.
2. Hockel M, Vaupel P. Tumor hypoxia: definitions and current clinical, biologic, and molecular aspects. *J Natl Cancer Inst.* 2001;93:266–276.
3. Evans SM, Koch CJ. Prognostic significance of tumor oxygenation in humans. *Cancer Lett.* 2003;195:1–16.
4. Rofstad EK, Danielsen T. Hypoxia-induced metastasis of human melanoma cells: involvement of vascular endothelial growth factor-mediated angiogenesis. *Br J Cancer.* 1999;80:1697–1707.
5. Nordsmark M, Overgaard M, Overgaard J. Pretreatment oxygenation predicts radiation response in advanced squamous cell carcinoma of the head and neck. *Radiother Oncol.* 1996;41:31–39.
6. Rofstad EK, Sundfor K, Lyng H, Trope CG. Hypoxia-induced treatment failure in advanced squamous cell carcinoma of the uterine cervix is primarily due to hypoxia-induced radiation resistance rather than hypoxia-induced metastasis. *Br J Cancer.* 2000;83:354–359.
7. Vaupel P, Hockel M, Mayer A. Detection and characterization of tumor hypoxia using pO_2 histography. *Antioxid Redox Signal.* 2007;9:1221–1235.
8. Smalley KS, Brafford PA, Herlyn M. Selective evolutionary pressure from the tissue microenvironment drives tumor progression. *Semin Cancer Biol.* 2005;15:451–459.
9. Evans SM, Du KL, Chalian AA, et al. Patterns and levels of hypoxia in head and neck squamous cell carcinomas and their relationship to patient outcome. *Int J Radiat Oncol Biol Phys.* 2007;69:1024–1031.
10. Kaanders JH, Wijffels KI, Marres HA, et al. Pimonidazole binding and tumor vascularity predict for treatment outcome in head and neck cancer. *Cancer Res.* 2002;62:7066–7074.
11. Olive PL, Banath JP, Aquino-Parsons C. Measuring hypoxia in solid tumours: is there a gold standard? *Acta Oncol.* 2001;40:917–923.
12. Krause BJ, Beck R, Souvatzoglou M, Piert M. PET and PET/CT studies of tumor tissue oxygenation. *Q J Nucl Med Mol Imaging.* 2006;50:28–43.
13. Lee ST, Scott AM. Hypoxia positron emission tomography imaging with ^{18}F-fluoromisonidazole. *Semin Nucl Med.* 2007;37:451–461.
14. Lehtio K, Oikonen V, Nyman S, et al. Quantifying tumour hypoxia with fluorine-18 fluoroerythronitroimidazole ([^{18}F]FETNIM) and PET using the tumour to plasma ratio. *Eur J Nucl Med Mol Imaging.* 2003;30:101–108.
15. Grosu AL, Souvatzoglou M, Roper B, et al. Hypoxia imaging with FAZA-PET and theoretical considerations with regard to dose painting for individualization of radiotherapy in patients with head and neck cancer. *Int J Radiat Oncol Biol Phys.* 2007;69:541–551.
16. Evans SM, Kachur AV, Shiue CY, et al. Noninvasive detection of tumor hypoxia using the 2-nitroimidazole [^{18}F]EF1. *J Nucl Med.* 2000;41:327–336.
17. Dolbier WR Jr, Li AR, Koch CJ, Shiue CY, Kachur AV. [^{18}F]-EF5, a marker for PET detection of hypoxia: synthesis of precursor and a new fluorination procedure. *Appl Radiat Isot.* 2001;54:73–80.
18. Koch CJ, Hahn SM, Rockwell K Jr, Covey JM, McKenna WG, Evans SM. Pharmacokinetics of EF5 [2-(2-nitro-1-H-imidazol-1-yl)-*N*-(2,2,3,3,3-pentafluoropropyl) acetamide] in human patients: implications for hypoxia measurements in vivo by 2-nitroimidazoles. *Cancer Chemother Pharmacol.* 2001;48:177–187.
19. Ziemer LS, Evans SM, Kachur AV, et al. Noninvasive imaging of tumor hypoxia in rats using the 2-nitroimidazole ^{18}F-EF5. *Eur J Nucl Med Mol Imaging.* 2003;30:259–266.
20. Evans SM, Fraker D, Hahn SM, et al. EF5 binding and clinical outcome in human soft tissue sarcomas. *Int J Radiat Oncol Biol Phys.* 2006;64:922–927.
21. Koch CJ. Measurement of absolute oxygen levels in cells and tissues using oxygen sensors and 2-nitroimidazole EF5. *Methods Enzymol.* 2002;352:3–31.
22. Evans SM, Hahn S, Pook DR, et al. Detection of hypoxia in human squamous cell carcinoma by EF5 binding. *Cancer Res.* 2000;60:2018–2024.
23. Evans SM, Judy KD, Dunphy I, et al. Comparative measurements of hypoxia in human brain tumors using needle electrodes and EF5 binding. *Cancer Res.* 2004;64:1886–1892.
24. Nordsmark M, Alsner J, Keller J, et al. Hypoxia in human soft tissue sarcomas: adverse impact on survival and no association with p53 mutations. *Br J Cancer.* 2001;84:1070–1075.
25. Bergman J, Solin O. Fluorine-18-labeled fluorine gas for synthesis of tracer molecules. *Nucl Med Biol.* 1997;24:677–683.
26. Blomqvist G. On the construction of functional maps in positron emission tomography. *J Cereb Blood Flow Metab.* 1984;4:629–632.
27. Meyer E. Simultaneous correction for tracer arrival delay and dispersion in CBF measurements by the $H_2{}^{15}O$ autoradiographic method and dynamic PET. *J Nucl Med.* 1989;30:1069–1078.
28. van den Hoff J, Burchert W, Muller-Schauenburg W, Meyer GJ, Hundeshagen H. Accurate local blood flow measurements with dynamic PET: fast determination of input function delay and dispersion by multilinear minimization. *J Nucl Med.* 1993;34:1770–1777.
29. Loening AM, Gambhir SS. AMIDE: a free software tool for multimodality medical image analysis. *Mol Imaging.* 2003;2:131–137.
30. Ljungkvist AS, Bussink J, Kaanders JH, van der Kogel AJ. Dynamics of tumor hypoxia measured with bioreductive hypoxic cell markers. *Radiat Res.* 2007;167:127–145.
31. Grönroos T, Tuomela J, Eskola O, et al. Biodistribution of the hypoxia marker ^{18}F-EF5 in mice bearing a prostate cancer tumour model [abstract]. *Eur J Nucl Med Mol Imaging.* 2004;31(suppl):S384.
32. Laughlin KM, Evans SM, Jenkins WT, et al. Biodistribution of the nitroimidazole EF5 (2-[2-nitro-^{1}H-imidazol-1-yl]-*N*-(2,2,3,3,3-pentafluoropropyl) acetamide) in mice bearing subcutaneous EMT6 tumors. *J Pharmacol Exp Ther.* 1996;277:1049–1057.
33. Lehtio K, Oikonen V, Gronroos T, et al. Imaging of blood flow and hypoxia in head and neck cancer: initial evaluation with [^{15}O]H_2O and [^{18}F]fluoroerythronitroimidazole PET. *J Nucl Med.* 2001;42:1643–1652.
34. Thorwarth D, Eschmann SM, Scheiderbauer J, Paulsen F, Alber M. Kinetic analysis of dynamic ^{18}F-fluoromisonidazole PET correlates with radiation treatment outcome in head-and-neck cancer. *BMC Cancer.* 2005;5:152.
35. Cherk MH, Foo SS, Poon AM, et al. Lack of correlation of hypoxic cell fraction and angiogenesis with glucose metabolic rate in non-small cell lung cancer assessed by ^{18}F-fluoromisonidazole and ^{18}F-FDG PET. *J Nucl Med.* 2006;47:1921–1926.
36. Becker A, Hansgen G, Bloching M, Weigel C, Lautenschlager C, Dunst J. Oxygenation of squamous cell carcinoma of the head and neck: comparison of primary tumors, neck node metastases, and normal tissue. *Int J Radiat Oncol Biol Phys.* 1998;42:35–41.
37. Rajendran JG, Schwartz DL, O'Sullivan J, et al. Tumor hypoxia imaging with [F-18] fluoromisonidazole positron emission tomography in head and neck cancer. *Clin Cancer Res.* 2006;12:5435–5441.
38. Evans SM, Hahn S, Judy KD, et al. ^{18}F EF5 PET imaging with immunohistochemical validation in patients with brain lesions [abstract]. *Int J Radiat Oncol Biol Phys.* 2006;66(suppl):S248.